NRL Memorandum Report 3650

Morphological Studies of Rising Equatorial Spread F Bubbles

S. L. OSSAKOW

Plasma Dynamics Branch
Plasma Physics Division

and

P. K. CHATURVEDI

University of Maryland
College Park, Maryland 20742

November 1977

This Research was sponsored in part by the Office of Naval Research and by the Defense Nuclear Agency under Subtask I25AAXYX960, work unit 06, Wideband Data.

NAVAL RESEARCH LABORATORY
Washington, D.C.

REPORT DOCUMENTATION PAGE

READ INSTRUCTIONS BEFORE COMPLETING FORM

1. REPORT NUMBER: NRL Memorandum Report 3650
2. GOVT ACCESSION NO.:
3. RECIPIENT'S CATALOG NUMBER:

4. TITLE (and Subtitle): MORPHOLOGICAL STUDIES OF RISING EQUATORIAL SPREAD F BUBBLES

5. TYPE OF REPORT & PERIOD COVERED: Interim report on a continuing NRL problem.

6. PERFORMING ORG. REPORT NUMBER:

7. AUTHOR(s): S. L. Ossakow and P. K. Chaturvedi*

8. CONTRACT OR GRANT NUMBER(s):

9. PERFORMING ORGANIZATION NAME AND ADDRESS: Naval Research Laboratory, Washington, D. C. 20305

10. PROGRAM ELEMENT, PROJECT, TASK AREA & WORK UNIT NUMBERS: NRL Problem No. H02-42D; DNA Subtask I25AAXYX960

11. CONTROLLING OFFICE NAME AND ADDRESS: Defense Nuclear Agency, Washington, D. C. 20305 and Office of Naval Research, Arlington, VA 22217

12. REPORT DATE: November 1977

13. NUMBER OF PAGES: 52

14. MONITORING AGENCY NAME & ADDRESS (if different from Controlling Office):

15. SECURITY CLASS. (of this report): UNCLASSIFIED

15a. DECLASSIFICATION/DOWNGRADING SCHEDULE:

16. DISTRIBUTION STATEMENT (of this Report)

Approved for public release; distribution unlimited.

17. DISTRIBUTION STATEMENT (of the abstract entered in Block 20, if different from Report)

18. SUPPLEMENTARY NOTES

This Research was sponsored in part by the Office of Naval Research and by the Defense Nuclear Agency under subtask I25AAXYX960, work unit 06 "Wideband Data".

*University of Maryland, College Park, Maryland

19. KEY WORDS (Continue on reverse side if necessary and identify by block number)

Collisional Rayleigh-Taylor Regime
Analytic Morphological Studies
Equatorial Spread F Bubbles
Rise Velocities

20. ABSTRACT (Continue on reverse side if necessary and identify by block number)

Analytical electrodynamic morphological studies of rising equatorial Spread F bubbles, within the context of the collisional Rayleigh-Taylor regime, are presented. The analogy between bubbles (plasma density depletions) and barium clouds (plasma density enhancements) is noted. Bubbles tend to steepen on their top and elongate in the vertical direction and they narrow horizontally as they rise through the equatorial F region ionosphere. Linear and nonlinear models of constant shape bubbles are presented. It is shown, for these models that the vertical bubble rise velocity, $V_B = (g/\upsilon_{in})f(\delta n/n_o)$, where υ_{in} is the ion-neutral collision frequency and f is an increasing

(Continues)

20. Abstract (Continued)

function of $\delta n/n_o$ (fractional density depletion), depending on the shape of the bubble. Consequently, high altitudes and/or large percentage plasma depletions yield large vertical bubble rise velocities. The models are extended to include arbitrary electric fields in addition to the gravitational force.

CONTENTS

MORPHOLOGICAL STUDIES OF RISING EQUATORIAL SPREAD F BUBBLES

I. INTRODUCTION

Recently, experimental (Kelley et al., 1976; Woodman and La Hoz, 1976; and McClure et al., 1977) and numerical simulation studies (Scannapieco and Ossakow, 1976) of the nighttime equatorial F region have given evidence for rising bubbles (plasma density depletions). The vertical speed of these bubbles has been observed (McClure et al., 1977) to range from very low (several meters/sec and even zero) to very high ($\sim$100 m/sec or more) velocities. Hudson [1977] has attempted to describe these rising bubbles within the context of the collisionless Rayleigh-Taylor mechanism using techniques in two dimensions that Chaturvedi and Kaw (1975 a,b) used in one dimension. Ott [1977] has described the rise of equatorial Spread F bubbles, in both the collisional and collisionless Rayleigh-Taylor regimes, by noting the analogy with bubbles in fluids. Szuszczewicz [1977] has discussed the chemistry and transport of equatorial Spread F ionospheric holes.

It has been pointed out (Scannapieco and Ossakow, 1976; and Scannapieco et al., 1976) that there is a considerable analogy between equatorial Spread F (in the collision-dominated regime) and barium cloud studies. Indeed barium clouds can be viewed as Pedersen conductivity or plasma density enhancements while natural equatorial Spread F bubbles (or artificially created ionospheric holes, e.g., see Mendillo et al.,

Note: Manuscript submitted November 7, 1977.

1975; and Bernhardt and da Rosa, 1977) can be viewed as Pedersen conductivity or plasma density depletions. In the present paper, we wish to discuss equatorial Spread F bubble shapes and vertical rise rates within the context of the collisional Rayleigh-Taylor regime (as invoked by Scannapieco and Ossakow, 1976), making use of the electrodynamic analogy (i.e., the electrical properties of the bubbles) with barium clouds. In section II we present the general theory, with subsections dwelling on linear and nonlinear bubble rise velocity models. Section III deals with the discussion and summary.

II. THEORY

The equations governing equatorial Spread F (within the context of the collisional Rayleigh-Taylor instability) are (see Scannapieco and Ossakow, 1976)

$$\frac{\partial n}{\partial t} + \nabla_\perp \cdot \left[\frac{nc}{B}\left(\frac{M}{e}\underline{g} \times \hat{b} - \nabla_\perp \psi \times \hat{b}\right)\right] = -\nu_R(n-n_o) \tag{1}$$

$$\nabla_\perp(\nu_{in} n \nabla_\perp \psi) = \frac{M}{e}\underline{g} \cdot \nabla_\perp(\nu_{in} n) + \frac{B}{c}(\underline{g} \times \hat{b}) \cdot \nabla_\perp n \tag{2}$$

where c is the speed of light, B the magnetic field (taken to be constant), e the electronic charge, M the mass of the ions, $\underline{g}$ acceleration of gravity, $\hat{b} = \underline{B}/|B|$ (pointing North), the subscript $\perp$ means perpendicular to $\hat{b}$ (Note: the geometry we will be employing for equatorial Spread F is such that x is upward, y is horizontal and eastward and z is northward and along the earth's magnetic field), ν_R is the recombination rate, n the ion number density (or equivalently a field line integrated number density in a slab geometry), $E = -\nabla\psi$, where ψ is the electrostatic potential (in this model there is no ambient, i.e., zero order, horizontal electric field), ν_{in} the ion-neutral collision

frequency (a function of altitude) and n_o the equilibrium ionospheric electron (ion) number density.

If we neglect recombination effects, neglect the variation of ν_{in} with altitude, and set $\psi = \phi_o + \phi$ (where from (1) and (2) $\nabla\phi_o = \frac{Mg}{e}$), then we have

$$\frac{\partial n}{\partial t} - \frac{c}{B} (\nabla_\perp \phi \times \hat{b}) \cdot \nabla_\perp n = 0 \tag{3}$$

$$\nabla_\perp \cdot (n \nabla_\perp \phi) = \frac{\Omega}{\nu_{in}} \frac{M}{e} \underline{g} \times \hat{b} \cdot \nabla_\perp n \tag{4}$$

(Note: The same potential equation (4) can be obtained by keeping terms of O(1) compared with ν_{in}/Ω, where $\Omega = eB/Mc$, in eq. (2)). The simplest set of equations describing F region barium cloud morphology and striations (for a one level model and in the $\underline{E}_o \times \underline{B}$ drift frame) is (see Perkins et al., 1973 and Zabusky et al., 1973)

$$\frac{\partial N}{\partial t} - \frac{c}{B} (\nabla_\perp \phi \times \hat{b}) \cdot \nabla_\perp N = 0 \tag{5}$$

$$\nabla_\perp (N \nabla_\perp \phi) = \underline{E}_o \cdot \nabla_\perp N \tag{6}$$

where $\underline{E}_o$ is taken to be the ambient electric field perpendicular to $\underline{B}$ ($\underline{E} \equiv \underline{E}_o - \nabla_\perp \phi$) and N is the magnetic field line integrated Pedersen

conductivity or equivalently the magnetic field line integrated plasma density. (Note: In these equations ν_{in} is taken to be a constant and so represents a rotated geometry, i.e., the barium cloud equations are more applicable to high latitudes where $\underline{B}$ is vertical, $\nabla_{\perp} N$ and $\underline{E}_0$ are horizontal.) If gravitational effects were also included in (6) then $\underline{E}^* \equiv \underline{E}_0 + (\Omega/\nu_{in})(M/e)\ \underline{g} \times \hat{b}$ would replace $\underline{E}_0$ on the right hand side of (6) (see Perkins et al., 1973). The two sets of equations (3) and (4), and (5) and (6) are essentially the same with $(\Omega/\nu_{in})(M/e)\ \underline{g} \times \hat{b}$ playing the role of an electric field in the potential eg. (4) (recall also the definition of $\underline{E}^*$).

Let us now discuss some depletion and enhancement cloud morphology. The separate coupled sets of equations (3) and (4) and (5) and (6) have no steady state solutions if the cloud, as described by n or N, has a finite size (with the gradient of n or N finite) in two dimensions perpendicular (x,y) to the magnetic field (see Perkins et al., 1973 and Dungey, 1958). Another result concerns the initial deformation of a cylindrical plasma density or Pedersen conductivity enhancement (barium cloud) and a cylindrical plasma density or Pedersen conductivity depletion (equatorial Spread F bubbles or artificially created ionospheric holes). The situation is illustrated in Figure 1. Here in this context eq. (4) or (6) is simply the problem of cylindrical dielectric immersed in a uniform electric field (where in the equatorial Spread F situation $(\Omega/\nu_{in})(M/e)\ \underline{g} \times \hat{b}$ plays the role of an equivalent electric field . In the case (A) of the density enhancement (e.g., barium cloud) the induced

electric field is opposed to the uniform electric field, $\underline{E}_0$, so that $\underline{E}'$, the total electric field inside the enhancement is less than $\underline{E}_0$. In the case (B) of the density depletion (e.g., equatorial Spread F bubble or artificially created "hole") the induced electric field is in the direction of the uniform electric field, $\underline{E}_0$, so that $\underline{E}'$, the total electric field inside the depletion is greater than $\underline{E}_0$. (Note: the formulas for $\underline{E}'$ are approximate and specific models will be discussed later on in the text.) It should be pointed out that in Fig. 1a the circles representing the isodensity contours are such that the enhancement and depletion are maximum in the center and fall off as one moves away from the center. In this way the induced electric field goes to zero outside of the enhancement or depletion (Note: for the enhancement the induced electric field is $-\delta N\underline{E}_0/(N_0 + \delta N)$, where N_0 is the ambient ionospheric density and δN is the enhanced density, while for the depletion the induced electric field is $\delta n\underline{E}_0/(n_0 - \delta n)$ where δn is the magnitude of the depletion and n_0 is the ambient density). In case (A) the $\underline{E}' \times \underline{B}$ drift of the center of the enhancement counteracts the general $\underline{E}' \times \underline{B}$ drift and the center of the enhancement (cloud) has the slowest drift. The backside (side opposite to $\underline{E}_0 \times \underline{B}$ motion) of the enhancement catches up with the center and a steep density gradient forms there (depicted in Fig. 1b). Similarly, the frontside elongates. The area enclosed by any isodensity contour remains constant during the motion and the maximum value of $|N|$ is a constant of the motion (incompressibility).

In case (B), the $\underline{E}' \times \underline{B}$ drift of the center of the depletion (bubble) acts in concert with the general $\underline{E}' \times \underline{B}$ drift and the center of the

depletion has the fastest drift. The center now catches up to the front-side and a steep density gradient forms there (depicted in Fig. 1b). In this case the so-called backside (using barium cloud terminology) elongates. In the context of eq. (3) and (4) in Fig. 1, the area enclosed by any isodensity contour remains constant during the motion and the maximum value of $|n|$ is a constant (incompressibility). In both the enhancement and depletion cases the density piles up in the direction formed by the induced electric field crossed with the magnetic field. In both cases where these steep gradients form instabilities should be generated. In some sense the density depletion can be likened to an "antibarium cloud." Within the context of Fig. 1 we have spoken about depletions in general and the general results apply to natural Spread F bubbles or artificially created ionospheric holes (using H_2O, H_2, or high explosives). Let us now specialize these results to equatorial Spread F bubbles. In this case, neglecting for the moment any horizontal ambient electric field, $\underline{E}_0$ in Fig. 1 is really $(\Omega M/e\nu_{in})\ \underline{g} \times \hat{b}$ and it is the polarization (induced) electric field (in the direction of $\underline{E}'$ and equal to $(\Omega M/e\nu_{in})$ $(\delta n/(n_0 - \delta n))\ \underline{g} \times \hat{b}$ which causes the bubble to rise with respect to the ionosphere via the local $\underline{E} \times \underline{B}$ convective drift motion. The picture exhibited in Fig. 1 for Spread F bubbles (using essentially eq. (4) which contains collisional Rayleigh-Taylor effects) shows that the bubbles spread more vertically than horizontally. This agrees with the radar observations [Woodman and La Hoz, 1976] and of course the numerical simulations [Scannapieco and Ossakow, 1976] which utilized eq. (1) and (2).

Linear Spread F Bubble Rise Velocity Model

Let us now look at Spread F bubble rise velocities for various bubble models. We will utilize eq. (4) and in our first case let us include a horizontal ambient electric field, $\underline{E}_o$, to show its effects. Then the equation becomes

$$\nabla_\perp (n \nabla_\perp \phi) = E^* \cdot \nabla_\perp n \tag{7}$$

$$E^* \equiv \underline{E}_o + \frac{\Omega}{\nu_{in}} \frac{M}{e} \underline{g} \times \hat{b}$$

Our first model will be a linearized model such that

$$n = n_o(x) + n_1 e^{i(ky-\omega t)} \tag{8}$$

$$\phi = \phi_1 e^{i(ky-\omega t)}$$

where $n_o(x)$ is the equilibrium altitude dependent density profile and subscript one refers to perturbed quantities. Substituting (8) into (7) and taking $\underline{E}_o$ to be in the y direction yields for the polarization potential

$$\phi_1 = -i \left(\frac{\Omega}{\nu_{in}} \frac{M}{e} g + E_o \right) \frac{1}{k} \frac{n_1}{n_o} \tag{9}$$

The bubble velocity is

$$\underline{V}_B = \frac{c}{B} \underline{E} \times \hat{b} \tag{10}$$

In eq. (10) we use $\underline{E} = -\nabla\phi_1 = -i\underline{k}\phi_1$ so that for the linear case $|V_B| = |cE/B| = |ck\phi_1/B|$ and we have for the vertical velocity ($\delta n \equiv n_1$)

$$V_B = \frac{\delta n}{n_o}\left(\frac{g}{\nu_{in}} + \frac{cE_o}{B}\right) \tag{11}$$

(Note: Here δn is positive and taken to mean the magnitude of the depletion.) It is interesting to note that adding $\underline{E}_o$ in the direction parallel (antiparallel) to $\underline{g} \times \hat{b}$ increases (decreases) the polarization field (as given by $-\nabla\phi_1$) and makes the bubbles rise faster (slower). The numerical simulations of Scannapieco and Ossakow [1976] did not have a horizontal electric field and adding one in the proper direction would make the bubble rise faster. However let us look at the effect of E_o. We wish to compare the two terms inside the parenthesis of eq. (11). If we assume $E_o \sim$ 1mV/m, B = 0.3 gauss then $cE_o/B \sim$ 33 m/sec. At 350 km altitude $g/\nu_{in} \sim$ 40 m/sec, whereas at 450 km $g/\nu_{in} \sim$ 220 m/sec. Thus we see that as one goes to higher altitudes E_o makes a more negligible contribution to the bubble rise velocity. Indeed, even if the electric field reverses, once the bubble gets to higher altitudes (decreasing ν_{in}) the bubble would keep rising. This bubble rising even after the electric field reverses has been seen experimentally [Kelley, private communication, 1976].

Neglecting E_o in eq. (11) we have

$$V_B = \frac{g}{\nu_{in}} \frac{\delta n}{n_o} \tag{12}$$

Using Fig. 2 for ν_{in} as a function of altitude, Fig. 3 depicts V_B as a function of altitude for various values of percentage depletions, $\delta n/n_o$ (large $\delta n/n_o$ represents usage of eq. (12) beyond the range of validity and perhaps represents a lower bound). Immediately it can be seen from this figure that large bubble velocities ($\sim$100 m/sec) requires large depletions and/or high altitudes.

Nonlinear Spread F Bubble Rise Velocity Model

In the case of a so-called sheet geometry in which we allow n and ϕ to be functions of y only, eq. (4) can be integrated once to yield

$$\frac{\partial \phi}{\partial y} = \left[1 - \frac{n_o}{n}\right] \frac{\Omega}{\nu_{in}} \frac{M}{e} g \tag{13}$$

where n_o is the ambient density outside the bubble. For this case the dimension of the bubble in the vertical direction is extremely long compared with its horizontal dimension. Using eq. (13), the vertical bubble rise velocity now becomes

$$V_B = \frac{\frac{\delta n}{n_o}}{1 - \frac{\delta n}{n_o}} \frac{g}{\nu_{in}} \tag{14}$$

where we have used $\underline{V}_B = -\frac{c}{B}\frac{\partial\phi}{\partial y}\hat{y} \times \hat{b}$ and $n = n_o - \delta n$ for a depletion. A peculiarity of this model is that $V_B \to \infty$ as $\delta n/n_o \to 1$, i.e.; for a 100% depletion. Fig. 4 shows the bubble rise velocity as a function of altitude for various vales of $\delta n/n_o$, using eq. (14) and values of ν_{in} depicted in Fig. 2. Here, as in Fig. 3, high altitudes and/or large depletions yield high vertical bubble velocities.

As we have stated previously, eq. (3) and (4) in general do not admit of a two dimensional ($\perp \underline{B}$) solution. However, there is a pathological case where one can obtain exact solutions and we will discuss this now. We write for the density

$$n(x,y) = n_o - n_D(x,y) \equiv n_o \left[1 - \frac{\delta n}{n_o} F(x,y)\right] \qquad (15)$$

where n_o is the ambient ionospheric density, n_D represents the depletion or bubble ($\delta n/n_o$ is the magnitude of the ratio of maximum depleted density to ambient density), and F describes the shape of depletion. If $n_D(x,y) \to 0$ as $x,y \to \infty$ and $\nabla_\perp n$ is finite then there is no equilibrium solution to eq. (3) and (4). However, if the depletion density is a constant and the shape of the density depletion contour is an ellipse described by

$$n_D = \delta n\, H\left[1 - \left(\frac{x}{a}\right)^2 - \left(\frac{y}{b}\right)^2\right]$$

[where H(x) is the Heaviside step function and a and b represent the vertical dimension (axis of the ellipse) and horizontal (east-west)

dimension respectively], then the electric field inside the depletion is a constant and the depletion (bubble) moves with constant velocity without changing its shape. This method was first employed by Linson [1972] for barium clouds (plasma density enhancements) where eq. (5) and (6) were utilized. (Note: In this case the minus signs in eq. (15) would become plus signs.) Indeed, eq. (4) or (6) can be thought of as the case of a dielectric immersed in a uniform electric field. However, the plasma depletion is analogous to the case of a cavity immersed in a dielectric with a uniform field (since the field is enhanced inside a depletion). The solution of the potential eq. (4) or (6) for the general elliptical shape can be found in Smythe [1950]. For the case of a plasma depletion described by eq. (4), with $\underline{g} \times \hat{b}$ in the y direction, we have for the polarization (induced) electric field

$$- \frac{\partial \phi}{\partial y} = \frac{\Omega}{\nu_{in}} \frac{Mg}{e} \left(\frac{a \frac{\delta n}{n_o}}{b + a \left(1 - \frac{\delta n}{n_o}\right)} \right) \tag{16}$$

with the attendant bubble rise velocity given by

$$V_B = \frac{g}{\nu_{in}} \left(\frac{a \frac{\delta n}{n_o}}{b + a \left(1 - \frac{\delta n}{n_o}\right)} \right) \tag{17}$$

(Note: In arriving at eq. (16) we have assumed ν_{in} to be a constant. This is a good approximation so long as the size of the depletion is small compared with an atmospheric scale height).

Now we will examine eq. (17) with respect to different shapes. For the case b << a, i.e., the sheet geometry, we obtain

$$V_B = \frac{g}{\nu_{in}} \frac{\frac{\delta n}{n_o}}{1 - \frac{\delta n}{n_o}}$$

which is eq. (14) as it should be. For a/b → 0, i.e., a slab case (uniform in the direction of $\underline{g} \times \hat{b}$), $V_B \to 0$ since the induced electric field goes to zero. When a = b (cylindrical case), we have

$$V_B = \frac{\frac{\delta n}{n_o}}{2 - \frac{\delta n}{n_o}} \frac{g}{\nu_{in}} \tag{18}$$

For $\delta n/n_o << 1$ eq. (18) yields $V_B = 1/2\ (g/\nu_{in})(\delta n/n_o)$ which is half the value given by the linear perturbation model (see eq. (12)). With $\delta n/n_o = 1$ (100% depletion), eq. (18) yields $V_B = g/\nu_{in}$. Fig. 5 shows the vertical bubble rise velocity for a cylindrical shape (as given by eq. (18)) and Fig. 6 exhibits the bubble rise velocity for an elliptical shape (a/b = 5) as a function of altitude for various values of $\delta n/n_o$, using values of ν_{in} depicted in Fig. 2.

III. DISCUSSION AND SUMMARY

Figures 3-6 depict vertical bubble (plasma depletion) rise velocities for various bubble models (shapes), for equatorial Spread F geometry, as a function of altitude and percentage depletions. Exceedingly high velocities can be attained, especially for the severely elongated models (e.g., sheet model in Fig. 4 and the elliptical model with a 5:1 axial ratio in Fig. 6). Table 1 shows the bubble rise velocity, in units of g/ν_{in}, as a function of fractional depleted plasma density for various bubble shapes. For all values of $\delta n/n_o$ (except at 1.0) the nonlinear cylindrical model gives a smaller velocity (see also eqs. (12) and (18)) than the linear model. The table also shows that the cylindrical bubble velocity for a given $\delta n/n_o$ is attained by the sheet model for a value of 1/2 $\delta n/n_o$ (see also eqs. (14) and (18)). An elliptical model with 10:1 axial ratio is also shown in Table 1. Except for $\delta n/n_o = 1$, it has already become fairly sheet-like. A common feature to all models is that the higher the altitude and/or the higher the density depletion, the higher the vertical rise velocity. This result is consistent with the recent satellite in situ measurements described by McClure et al. [1977].

The models described by Fig. 3-6 essentially assume that the bubble does not change its shape. For real bubbles, where the depletion density changes inside the bubble, the bubble should elongate in the vertical direction (steepening on the topside of the bubble) and become narrower in the east-west extent. This is in agreement with the radar

observations (Woodman and La Hoz, 1976) and the numerical simulation of rising equatorial Spread F bubbles (Scannapieco and Ossakow, 1976). Therefore, in modeling a changing bubble by one of constant shape we are employing somewhat of an artifact. However, using this technique Linson [1972] has shown (using optical data) that evolving barium clouds (plasma density enhancements) tend to be more cylindrical than sheet-like. Using the constant shape approach and the simulation results of Scannapieco and Ossakow [1976], where $V_B \sim 10$ m/sec and $\delta n/n_o \sim 40\%$ for an altitude of 350 km, the cylindrical bubble shape is favored (although the simulation pictures show an elongated bubble). More data and simulation results are needed to ascertain which model fits best.

All of the models described in this paper, based on collisional Rayleigh-Taylor type equations, show that the vertical bubble rise velocity is of the form

$$V_B = \frac{g}{\nu_{in}} \; f\left(\frac{\delta n}{n_o}\right) \tag{19}$$

where $f(\delta n/n_o)$ is some function of $\delta n/n_o$. The factor g/ν_{in} should not be too surprising since the growth rate (γ) for the collisional Rayleigh-Taylor instability, neglecting recombination effects, is g/ν_{in} L (Hudson and Kennel, 1975; Scannapieco and Ossakow, 1976), which is a velocity divided by the electron density gradient scale length. This of course is similar to the growth rate ($\gamma = cE_o/BL$) for barium cloud striations

due to $\underline{E}_o \times \underline{B}$ gradient drift instability (Simon, 1963; Linson and Workman, 1970). This similarity between the gravitational and the electric field terms has been shown in eq. (11). In eq. (19), the factor g/ν_{in} favors high altitude because ν_{in} decreases as a function of altitude (see Fig. 2). The factor f increases with increasing $\delta n/n_o$ (see Fig. 3-6). At least according to linear theory, $\delta n/n_o$ increases with altitude and decreasing bottomside electron density gradient scale length ($\gamma = g/\nu_{in} L$). These ideas indicate that there is a range of bubble vertical rise velocities (in accord with McClure et al., [1977]), but these rise velocities depend on ambient equatorial F region ionospheric conditions (e.g., height of the F peak and bottomside gradient scale length). Recent numerical simulations (S. Ossakow, S. Zalesak and B. E. McDonald, private communication, 1977) support these ideas. Also, it should be pointed out that for $\delta n/n_o = 0$, i.e., for bubbles which have the same density as the background ionosphere, the induced (polarization) electric field (which causes the bubble to rise through $\underline{E} \times \underline{B}$) becomes zero (with all models, as it should), as does the attendant vertical bubble rise velocity. This simply states that a bubble created on the bottomside of the F region will rise until its density equals the topside background ionospheric density.

It should be pointed out that our vertical velocity result for cylindrical bubbles does not agree with Ott's [1977] result. In his analogy with bubbles in a fluid, Ott found only a cylindrical solution. For the collision dominated regime he found $V_B = 1/2(g/\nu_{in})(\delta n/n_o)$, in

our terminology; whereas, our result shows $V_B = 1/2(g/\nu_{in})(\delta n/n_o) \cdot (1 - 1/2(\delta n/n_o))^{-1}$. For the case where the bubble density is negligibly small ($\delta n/n_o \approx 1$) compared with the density in the ionosphere outside, Ott's result yields $V_B = 1/2(g/\nu_{in})$; whereas, our result yields $V_B = g/\nu_{in}$.

Finally some comments about the various upward and westward bubble velocities presented by McClure et al. [1977] and the tilts of the plumes seen by the Jicamarca radar measurements (Woodman and La Hoz, 1976). Equations (1) and (2), used by Scannapieco and Ossakow [1976], or eqs. (3) and (4) for that matter produce only vertical bubble rise. These equations only admit of a horizontal polarization electric field (eastward) caused by the $\underline{g} \times \hat{b}$ term such that depletions rise and enhancements fall with respect to the ionosphere. Inclusion of an ambient background horizontal electric field (eastward or westward) in the equations could only cause additional vertical (upward or downward) motion of the bubbles. Since the ionosphere moves mainly downward at night (westward electric field; see McClure et al., 1977) this could slow down the bubbles at low altitudes and have a negligible effect at higher altitudes (see eq. (11)). Vertically the bubbles move more slowly at lower altitudes and/or small values of $\delta n/n_o$. Thus there exist conditions whereby the bubbles do not move vertically with respect to the ionosphere. McClure et al. [1977] and Woodman and La Hoz [1976] have stated that the ionosphere moves mainly eastward at night. This would mean an ambient electric field pointing downward. Inclusion of such an

electric field in the equations would cause bubbles to move eastward. Thus the westward motion of the bubbles must be caused by introducing an asymmetry into the eq. (1) and (2) (or (3) and (4)) which causes a vertical (upward) electric field. Such an effect can be produced by an eastward directed neutral wind which would essentially polarize the bubble to produce an upward polarization electric field and account for the westward motion of the bubble (and tilts of the radar plumes). This last idea has also been set forth by Woodman and La Hoz [1976] and Ott [1977].

Recalling our discussion about the electric field, $E^* \equiv \underline{E}_o + (\Omega/\nu_{in})$. $(M/e)\ \underline{g} \times \hat{b}$, after eq. (6), all of our vertical bubble rise velocities can take account of horizontal motions. The general bubble velocity is then just $\underline{V}_B = (c/B)\ \underline{E}^* \times \hat{b}\ f(\delta n/n_o) = ((c/B)\ \underline{E}_o \times \hat{b} - \underline{g}/\nu_{in})\ f(\delta n/n_o)$. This clearly shows how the directionality of $\underline{V}_B$ is formed. In this case for the elliptical shape a is in the direction of $\underline{E}^* \times \hat{b}$, etc. and non-constant density depletions will steepen and elongate in this direction.

Recent results from the Wideband associated equatorial experiments performed at Kwajalein (August 1977) lend credence to this notion (S. Ossakow and J. Clark, private communication, 1977). Backscatter irregularity ($\sim$1 meter) measurements (performed by D. Towle) have shown that these patches rise and appear westward when neutral wind measurements (Fabry-Perot interferometer measurements performed by M. Biondi and D. Sipler) show strong west to east winds ($\sim$160 m/sec) earlier in the evening. As the evening progresses the neutral winds die down ($\sim$10-20 m/sec) and the radar shows the irregularities appearing eastward.

IV. ACKNOWLEDGMENT

This work was supported by the Defense Nuclear Agency and the Office of Naval Research.

Table 1. Bubble rise velocity (in units of g/ν_{in}), V_B', as a function of fractional depleted density, $\delta n/n_o$, for various bubble shapes.

V_B' \ $\frac{\delta n}{n_o}$	.25	.5	.75	.9	1
Linear	.25	.5	.75	.9	1
Sheet	.33	1	3	9	∞
Cylindrical	.14	.33	.6	.82	1
Elliptical (5:1)	.26	.71	1.67	3	5
Elliptical (10:1)	.29	.83	2.14	4.5	10

V. REFERENCES

Bernhardt, P., and A. V. da Rosa, A refracting radio telescope, Radio Sci. 12, 327, 1977.

Chaturvedi, P. K., and P. K. Kaw, Steady state finite amplitude Rayleigh-Taylor modes in Spread F, Geophys. Res. Letts., 2, 381, 1975a.

Chaturvedi, P. K., and P. K. Kaw, Correction, Geophys. Res. Letts., 2, 499, 1975b.

Dungey, J. W., Cosmic Electrodynamics, p. 161, Cambridge University Press, London, 1958.

Hudson, M. K., Spread F Bubbles: Nonlinear Rayleigh-Taylor mode in two dimensions, J. Geophys. Res. (submitted 1977).

Hudson, M. K., and C. F. Kennel, Linear theory of equatorial Spread F, J. Geophys. Res., 80, 4581, 1975.

Kelley, M. C., G. Haerendel, H. Kappler, A. Valenzuela, B. B. Balsley, D. A. Carter, W. L. Ecklund, C. W. Carlson, B. Hausler, and R. Torbert, Evidence for a Rayleigh-Taylor type instability and upwelling of depleted density regions during equatorial Spread F, Geophys. Res. Letts., 3, 448, 1976.

Linson, L. M., Motion of barium ion clouds, Analysis of Barium Clouds - Semi-Annual Technical Report, RADC-TR-72-103, Vol. I, Avco Everett Reserach Laboratory, Everett, Mass., January 1972.

Linson, L. M., and J. B. Workman, Formation of striations in ionospheric plasma clouds, J. Geophys. Res., 75, 3211, 1970.

Mendillo, M., G. S. Hawkings, and J. A. Klobuchar, A sudden vanishing of the ionospheric F region due to the launch of Skylab, J. Geophys. Res., 80, 2217, 1975.

McClure, J. P., W. B. Hanson, and J. H. Hoffman, Plasma bubbles and irregularities in the equatorial ionosphere, J. Geophys. Res., 82, 2650, 1977.

Ott, E., Theory of Rayleigh-Taylor bubbles in the equatorial ionosphere, J. Geophys. Res. (submitted 1977).

Perkins, F. W., N. J. Zabusky, and J. H. Doles III, Deformation and striation of plasma clouds in the ionosphere, 1, J. Geophys. Res., 78, 697, 1973.

Scannapieco, A. J., and S. L. Ossakow, Nonlinear equatorial Spread F, Geophys. Res. Letts., 3, 451, 1976.

Scannapieco, A. J., S. L. Ossakow, S. R. Goldman, and J. M. Pierre, Plasma cloud late time striation spectra, J. Geophys. Res., 81, 6037, 1976.

Simon, A., Instability of a partially ionized plasma in crossed electric and magnetic fields, Phys. Fluids, 6, 382, 1963.

Smythe, W. R., Static and Dynamic Electricity, p. 95, McGraw Hill, New York, 1950.

Szuszczewicz, E. P., Ionospheric holes and equatorial spread F: chemistry and transport, NRL Memo Report 3554, July 1977 (also submitted for publication in JGR).

Woodman, R. F., and C. La Hoz, Radar observations of F region equatorial irregularities, J. Geophys. Res., 81, 5447, 1976.

Zabusky, N. J., J. H. Doles III, and F. W. Perkins, Deformation and striation of plasma clouds in the ionosphere, 2, numerical simulation of a nonlinear two-dimensional model, J. Geophys. Res., 78, 711, 1973.

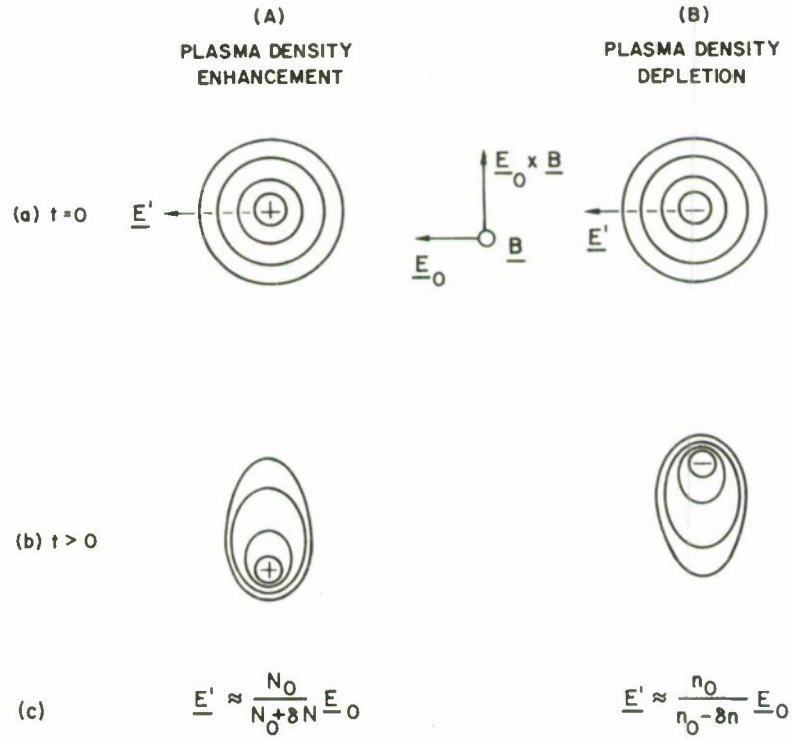

Fig. 1 — Deformation of (A) a plasma density enhancement (e.g., a barium cloud) and (B) a plasma density depletion (e.g., equatorial Spread F bubble or artificially created "hole") in crossed electric ($\underline{E}_o$) and magnetic ($\underline{B}$) fields (representative of equatorial geometry). (a) Initial (t=0) cylindrical isodensity contours with largest enhancement (+) and depletion (-) values in the center and falling off away from these values to an ambient level n_o outside. $\underline{E}'$ represents the total electric field inside the enhancement or depletion and $\underline{E}_o$ is the ambient field outside. (b) Qualitative evolution of the isodensity contours. (c) Approximate values for the initial electric field ($\underline{E}'$) inside the enhancement or depletion.

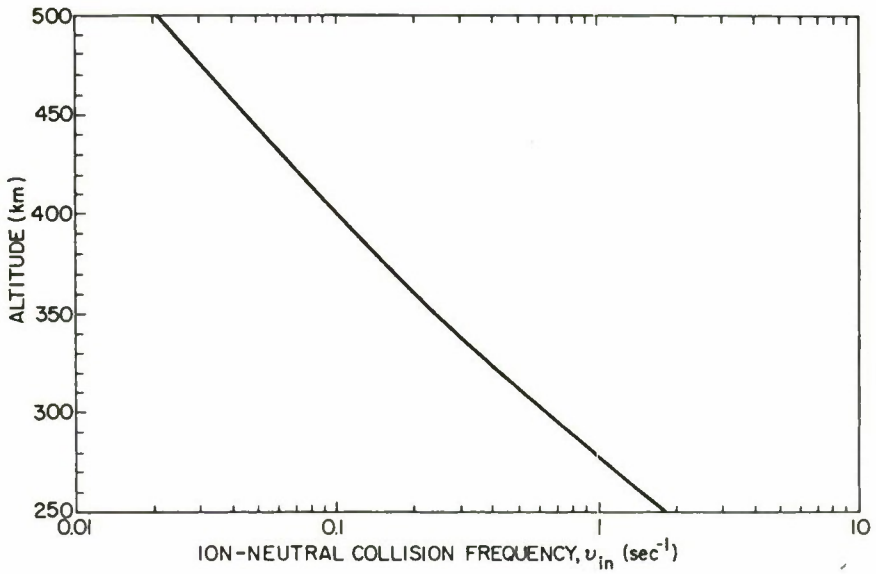

Fig. 2 — Ion-neutral collision frequency, υ_{in}, as a function of altitude

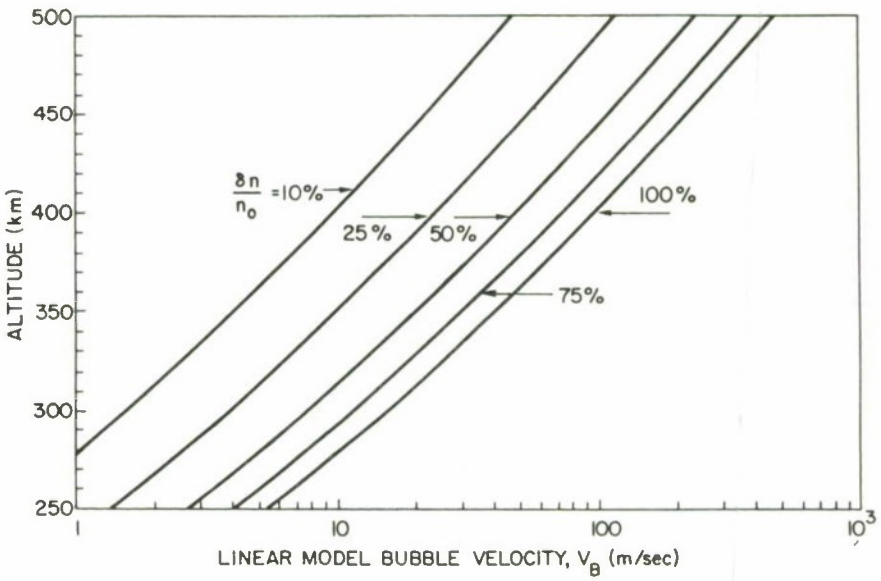

Fig. 3 — Depletion (bubble) vertical rise velocity, V_B, as a function of altitude for various values of the percentage depletion, $\delta n/n_o$, for the linear bubble model, i.e., $V_B = (g/\upsilon_{in})(\delta n/n_o)$

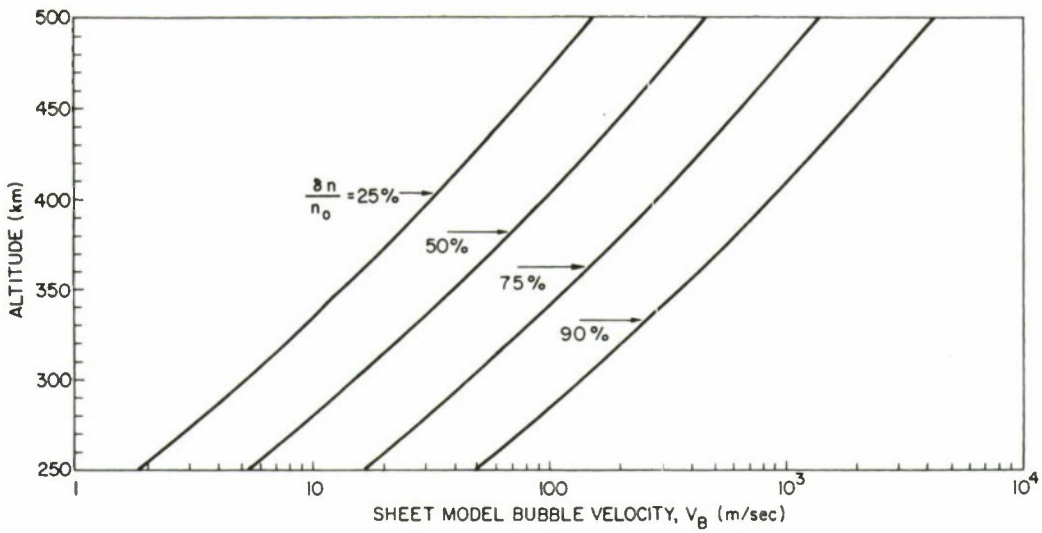

Fig. 4 — Same as fig. 3, but for the nonlinear sheet bubble model, i.e., $V_B = (g/\upsilon_{in})(\delta n/n_o)(1-\delta n/n_o)^{-1}$

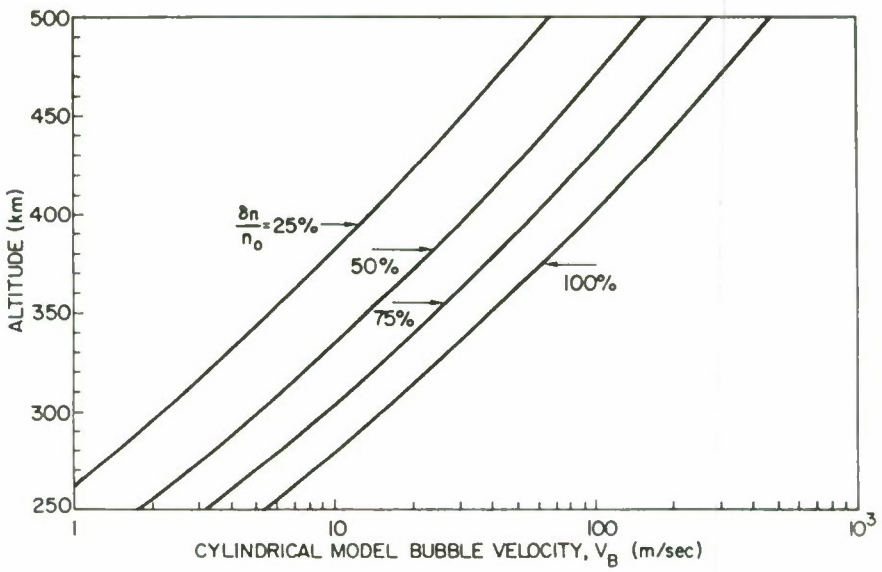

Fig. 5 — Same as fig. 3, but for the nonlinear cylindrical bubble model, i.e., $V_B = (g/\upsilon_{in})(\delta n/n_o)(2-\delta n/n_o)^{-1}$

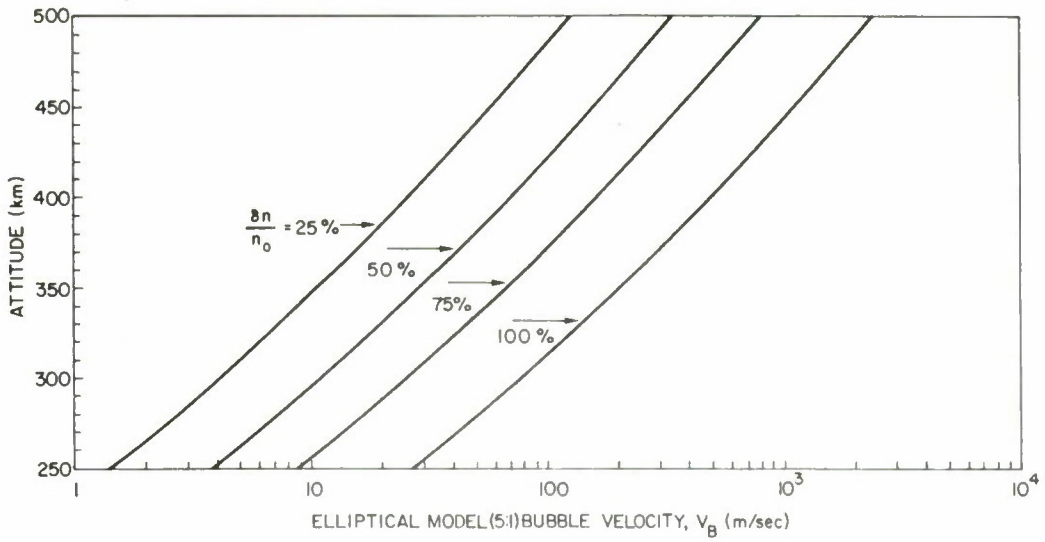

Fig. 6 — Same as fig. 3, but for the nonlinear elliptical bubble model (with the vertical dimension five times the horizontal dimension), i.e., $V_B = (g/\upsilon_{in})(5\ \delta n/n_o)(6\text{-}5\ \delta n/n_o)^{-1}$

DISTRIBUTION LIST

DEPARTMENT OF DEFENSE

DIRECTOR
COMMAND CONTROL TECHNICAL CENTER
PENTAGON RM BE 685
WASHINGTON, D.C. 20301
01CY ATTN C-650 G. C. JONES
01CY ATTN C-650 W. HEIDIG
01CY ATTN C-312 R. MASON

DIRECTOR
DEFENSE ADVANCED RSCH PROJ AGENCY
ARCHITECT BUILDING
1400 WILSON BLVD.
ARLINGTON, VA. 22209
01CY ATTN NUCLEAR MONITORING RESEARCH
01CY ATTN STRATEGIC TECH OFFICE

DEFENSE COMMUNICATION ENGINEER CENTER
1860 WIEHLE AVENUE
RESTON, VA. 22090
01CY ATTN CODE R820 R. L. CRAWFORD
01CY ATTN CODE R410 JAMES W. MCLEAN

DIRECTOR
DEFENSE COMMUNICATIONS AGENCY
WASHINGTON, D.C. 20305
(ADR CNWDI: ATTN CODE 240 FOR)
01CY ATTN CODE 480
01CY ATTN CODE 810 R. W. ROSTRON
01CY ATTN CODE 101B MAJ R. ROOD
01CY ATTN MAUREY RAFFENSPERGER

DEFENSE DOCUMENTATION CENTER
CAMERON STATION
ALEXANDRIA, VA. 22314
(12 COPIES IF OPEN PUBLICATION, OTHERWISE 2 COPIES)
12CY ATTN TC

DIRECTOR
DEFENSE INTELLIGENCE AGENCY
WASHINGTON, D.C. 20301
01CY ATTN DT-1B
01CY ATTN W. WITTIG DC-7D

DIRECTOR
DEFENSE NUCLEAR AGENCY
WASHINGTON, D.C. 20305
01CY ATTN STSI ARCHIVES
01CY ATTN STVL
03CY ATTN STTL TECH LIBRARY
01CY ATTN DDST
03CY ATTN RAAE

DIR OF DEFENSE RSCH & ENGINEERING
DEPARTMENT OF DEFENSE
WASHINGTON, D.C. 20301
01CY ATTN S&SS (OS)

COMMANDER
FIELD COMMAND
DEFENSE NUCLEAR AGENCY
KIRTLAND AFB, NM 87115
01CY ATTN FCPR

DIRECTOR
INTERSERVICE NUCLEAR WEAPONS SCHOOL
KIRTLAND AFB, NM 87115
01CY ATTN DOCUMENT CONTROL

DIRECTOR
JOINT STRAT TGT PLANNING STAFF JCS
OFFUTT AFB
OMAHA, NB 68113
01CY ATTN JLTW-2
01CY ATTN JPST CAPT G. D. GOETZ

CHIEF
LIVERMORE DIVISION FLD COMMAND DNA
LAWRENCE LIVERMORE LABORATORY
P. O. BOX 808
LIVERMORE, CA 94550
01CY ATTN FCPRL

DIRECTOR
NATIONAL SECURITY AGENCY
FT. GEORGE G. MEADE, MD 20755
01CY ATTN JOHN SKILLMAN R52
01CY ATTN FRANK LEONARD
01CY ATTN W14 PAT CLARK

OJCS/J-3
THE PENTAGON
WASHINGTON, D.C. 20301
(OPERATIONS)
01CY ATTN WWMCCS EVAL OFC MR. TOMA

ASD (C31) (SYSTEMS)
3D224, THE PENTAGON
WASHINGTON, D.C. 20301
01CY ATTN DR. M. EPSTEIN
01CY DR. J. BABCOCK

WWMCCS SYSTEM ENGINEERING ORG
WASHINGTON, D.C. 20305
01CY ATTN R. L. CRAWFORD

COMMANDER/DIRECTOR
ATMOSPHERIC SCIENCES LABORATORY
U.S. ARMY ELECTRONICS COMMAND
WHITE SANDS MISSILE RANGE, NM 88002
01CY ATTN DRSEL-BL-SY-S F. E. NILES

DIRECTOR
BMD ADVANCED TECH CTR
HUNTSVILLE OFFICE
P. O. BOX 1500
HUNTSVILLE, AL 35807
01CY ATTN ATC-T MELVIN T. CAPPS
01CY ATTN ATC-O W. DAVIES
01CY ATTN ATC-R DON RUSS

PROGRAM MANAGER
BMD PROGRAM OFFICE
5001 EISENHOWER AVENUE
ALEXANDRIA, VA 22333
01CY ATTN DACS-BMT JOHN SHEA

CHIEF C-E SERVICES DIVISION
U.S. ARMY COMMUNICATIONS CMD
PENTAGON RM 1B269
WASHINGTON, D.C. 20310
01CY ATTN CC-OPS-CE

COMMANDER
HARRY DIAMOND LABORATORIES
2800 POWDER MILL ROAD
ADELPHI, MD 20783
(CNWDI-INNER ENVELOPE: ATTN: DRXDO-RBH)
01CY ATTN MILDRED H. WEINER DRXDO-TI
01CY ATTN DRXDO-RB ROBERT WILLIAMS
01CY ATTN DRXDO-NP FRANCIS N. WIMENITZ
01CY ATTN DRXDO-NP CYRUS MOAZED

DIRECTOR
TRASANA
WHITE SANDS MISSILE RANGE, NM 88002
01CY ATTN ATAA-SA
01CY ATTN TCC/F. PAYAN JR
01CY ATTN ATAA-TAC LTC JOHN HESSE

COMMANDER
U.S. ARMY COMM-ELEC ENGRG INSTAL AGY
FT. HUACHUCA, AZ 85613
01CY ATTN EED-PED GEORGE LANE

COMMANDER
U.S. ARMY ELECTRONICS COMMAND
FORT MONMOUTH, NJ 07703
01CY ATTN DRSEL-NL-RD H. S. BENNET
01CY ATTN DRSEL-PL-ENV HANS A. BOMKE

COMMANDER
U.S. ARMY FOREIGN SCIENCE & TECH CTR
220 7TH STREET, NE
CHARLOTTESVILLE, VA 22901
01CY ATTN P. A. CROWLEY
01CY ATTN R. JONES

COMMANDER
U.S. ARMY MATERIEL DEV & READINESS CMD
5001 EISENHOWER AVENUE
ALEXANDRIA, VA 22333
01CY ATTN DRCLDC J. A. BENDER

COMMANDER
U.S. ARMY NUCLEAR AGENCY
FORT BLISS, TX 79916
01CY ATTN MONA-WE J. BERBERET

DIRECTOR
U.S. ARMY BALLISTIC RESEARCH LABS
ABERDEEN PROVING GROUND, MD 21005
01CY ATTN LAWRENCE J. PUCKETT

COMMANDER
U.S. ARMY SATCOM AGENCY
FT. MONMOUTH, NJ 07703
01CY ATTN DOCUMENT CONTROL

COMMANDER
U.S. ARMY MISSILE INTELLIGENCE AGENCY
REDSTONE ARSENAL, AL 35809
01CY ATTN JIM GAMBLE

CHIEF OF NAVAL OPERATIONS
NAVY DEPARTMENT
WASHINGTON, D.C. 20350
01CY ATTN OP 943 LCDR HUFF
01CY ATTN ALEXANDER BRANDT
01CY ATTN RONALD E. PITKIN

CHIEF OF NAVAL RESEARCH
NAVY DEPARTMENT
ARLINGTON, VA 22217
01CY ATTN CODE 418
01CY ATTN CODE 461

COMMANDER
NAVAL ELECTRONIC SYSTEMS COMMAND
NAVAL ELECTRONIC SYSTEMS CMD HQS
WASHINGTON, D.C. 20360
01CY ATTN NAVALEX 034 T BARRY HUGHES
01CY ATTN PME 117-T SATELLITE COMM PROJECT OFF
01CY ATTN PME 117

COMMANDING OFFICER
NAVAL INTELLIGENCE SUPPORT CTR
4301 SUITLAND ROAD, BLDG. 5
WASHINGTON, D.C. 20390
01CY ATTN MR. DUBBIN STIC 12

COMMANDER
NAVAL OCEAN SYSTEMS CENTER
SAN DIEGO, CA 92152
01CY ATTN WILLIAM F. MOLER
01CY ATTN CODE 0230 C. BAGGETT
03CY ATTN CODE 2200
01CY ATTN R. EASTMAN

DIRECTOR
NAVAL RESEARCH LABORATORY
WASHINGTON, D.C. 20375
01CY ATTN CODE 7700 TIMOTHY P. COFFEY
03CY ATTN CODE 7701 JACK D. BROWN
01CY ATTN CODE 7750
01CY ATTN CODE 5400 BRUCE WALD
03CY ATTN CODE 5450 TELECOMMUNICATIONS SYSTEMS TECH.

COMMANDER
NAVAL SPACE SURVEILLANCE SYSTEM
DAHLGREN, VA 22448
01CY ATTN CAPT J. H. BURTON

COMMANDER
NAVAL SURFACE WEAPONS CENTER
WHITE OAK, SILVER SPRING, MD 20910
01CY ATTN CODE WA501 NAVY NUC PRGMS OFF

DIRECTOR
STRATEGIC SYSTEMS PROJECT OFFICE
NAVY DEPARTMENT
WASHINGTON, D.C. 20376
01CY ATTN NSP-2141
01CY ATTN NSSP-2722 FRED WIMBERLY

NAVAL SPACE SYSTEM ACTIVITY
P. O. BOX 92960
WORLDWAY POSTAL CENTER
LOS ANGELES, CALIF. 90009
01CY ATTN A. B. HAZZARD

COMMANDER
ADC/DC
ENT AFB, CO 80912
01CY ATTN DC MR. LONG

COMMANDER
ADCOM/XPD
ENT AFB, CO 80912
01CY ATTN XPQDQ

AF GEOPHYSICS LABORATORY, AFSC
HANSCOM AFB, MA 01731
01CY ATTN OPR HAROLD GARDNER
01CY ATTN OPR JAMES C. ULWICK
01CY ATTN LKB KENNETH S. W. CHAMPION
01CY ATTN OPR ALVA T. STAIR
01CY ATTN SUOL RSCH LIB
01CY ATTN PHP JULES AARONS
01CY ATTN PHD JURGEN BUCHAU
01CY ATTN PHD JOHN P. MULLEN

AF WEAPONS LABORATORY, AFSC
KIRTLAND AFB, NM 87117
01CY ATTN SUL
01CY ATTN CA ARTHUR H. GUENTHER
01CY ATTN DYC CAPT L. WITTWER
01CY ATTN SAS JOHN M. KAMM
01CY ATTN DYC CAPT MARK A. FRY

AFTAC
PATRICK AFB, FL 32925
01CY ATTN TF/MAJ WILEY
01CY ATTN TN

AIR FORCE AVIONICS LABORATORY, AFSC
WRIGHT-PATTERSON AFB, OH 45433
01CY ATTN AAD WADE HUNT
01CY ATTN AFAL AAB H. M. HARTMAN
01CY ATTN AAD ALLEN JOHNSON

HEADQUARTERS
ELECTRONIC SYSTEMS DIVISION/XR
HANSCOM AFB, MA 01731
01CY ATTN XRC LTC J. MORIN
01CY ATTN XRE LT MICHAELS

HEADQUARTERS
ELECTRONIC SYSTEMS DIVISION/YS
HANSCOM AFB, MA 01731
01CY ATTN YSEV

COMMANDER
FOREIGN TECHNOLOGY DIVISION, AFSC
WRIGHT-PATTERSON AFB, OH 45433
01CY ATTN NICD LIBRARY
01CY ATTN ETD B. L. BALLARD

HQ USAF/RD
WASHINGTON, D.C. 20330
01CY ATTN RDQ

COMMANDER
ROME AIR DEVELOPMENT CENTER, AFSC
GRIFFISS AFB, NY 13440
01CY ATTN EMTLD DOC LIBRARY
01CY ATTN OCSE V. COYNE

SAMSO/SZ
POST OFFICE BOX 92960
WORLDWAY POSTAL CENTER
LOS ANGELES, CA 90009
(SPACE DEFENSE SYSTEMS)
01CY ATTN SZJ MAJOR LAWRENCE DOAN

COMMANDER IN CHIEF
STRATEGIC AIR COMMAND
OFFUTT AFB, NB 68113
01CY ATTN XPFS MAJ BRIAN G. STEPHAN
01CY ATTN ADWATE CAPT BRUCE BAUER
01CY ATTN NRT

HEADQUARTERS
ELECTRONIC SYSTEMS DIVISION (AFSC)
HANSCOM AFB, MA 01731
01CY ATTN JIM DEAS

SAMSO/YA
P. O. BOX 92960
WORLDWAY POSTAL CENTER
LOS ANGELES, CA 90009
01CY ATTN YAT CAPT L. BLACKWELDER

SAMSO/SK
P. O. BOX 92960
WORLDWAY POSTAL CENTER
LOS ANGELES, CA 90009
01CY ATTN SKA LT MARIA A. CLAVIN

SAMSO/MN
NORTON AFB, CA 92419
(MINUTEMAN)
01CY ATTN MNNL LTC KENNEDY

COMMANDER
ROME AIR DEVELOPMENT CENTER, AFSC
HANSCOM AFB, MA 01733
01CY ATTN ETEI A. LORENTZEN

EG&G, INC.
LOS ALAMOS DIVISION
P. O. BOX 809
LOS ALAMOS, NM 85544
01CY ATTN JAMES R. BREEDLOVE

UNIVERSITY OF CALIFORNIA
LAWRENCE LIVERMORE LABORATORY
P. O. BOX 808
LIVERMORE, CA 94550
01CY ATTN TECH INFO DEPT L-3
01CY ATTN RONALD L. OTT L-531
01CY ATTN DONALD R. DUNN L-156
01CY ATTN RASPH S. HAGER L-31

LOS ALAMOS SCIENTIFIC LABORATORY
P. O. BOX 1663
LOS ALAMOS, NM 87545
01CY ATTN DOC CON FOR ERIC LINDMAN
01CY ATTN DOC CON FOR R. F. TASCHEK
01CY ATTN DOC CON FOR ERIC JONES
01CY ATTN DOC CON FOR JOHN S. MALIK
01CY ATTN DOC CON FOR MARTIN TIERNEY J-10
01CY ATTN DOC CON FOR JOHN ZINN

SANDIA LABORATORIES
P. O. BOX 5800
ALBUQUERQUE, NM 87115
01CY ATTN DOC CON FOR J. P. MARTIN ORG 1732
01CY ATTN DOC CON FOR W. D. BROWN ORG 1353
01CY ATTN DOC CON FOR A. DEAN THORNBROUGH ORG 1245
01CY ATTN DOC CON FOR T. WRIGHT
01CY ATTN DOC CON FOR D. A. DAHLGREN ORG 1722

OTHER GOVERNMENT

DEPARTMENT OF COMMERCE
OFFICE OF TELECOMMUNICATIONS
INSTITUTE FOR TELECOM SCIENCE
BOULDER, CO 80302
01CY ATTN WILLIAM F. UTLAUT
01CY ATTN G. REED

NATIONAL OCEANIC & ATMOSPHERIC ADMIN
ENVIRONMENTAL RESEARCH LABORATORIES
DEPARTMENT OF COMMERCE
BOULDER, CO 80302
01CY ATTN JOSEPH H. POPE
01CY ATTN RICHARD GRUBB
01CY ATTN C. L. RUFENACH

NASA
GODDARD SPACE FLIGHT CENTER
GREENBELT, MD 20771
01CY ATTN ATS-6 OFC P. CORRIGAN

DEPARTMENT OF DEFENSE CONTRACTORS

AEROSPACE CORPORATION
P. O. BOX 92957
LOS ANGELES, CA 90009
01CY ATTN IRVING M. GARFUNKEL
01CY ATTN T. M. SALMI
01CY ATTN V. JOSEPHSON
01CY ATTN S. P. BOWER
01CY ATTN N. D. STOCKWELL
01CY ATTN P. P. OLSEN 120 RM 2224E
01CY ATTN F. E. BOND RM 5003
01CY ATTN J. E. CARTER 120 RM 2209
01CY ATTN F. A. MORSE A6 RM 2407

ANALYTICAL SYSTEMS ENGINEERING CORP
5 OLD CONCORD ROAD
BURLINGTON, MA 01803
01CY ATTN RADIO SCIENCES

BOEING COMPANY, THE
P. O. BOX 3707
SEATTLE, WA 98124
01CY ATTN GLEN KEISTER
01CY ATTN D. MURRAY

CALIFORNIA AT SAN DIEGO, UNIV OF
3175 MIRAMAR ROAD
LA JOLLA, CA 92037
01CY ATTN HENRY G. BOOKER

BROWN ENGINEERING COMPANY, INC.
CUMMINGS RESEARCH PARK
HUNTSVILLE, AL 35807
01CY ATTN ROMEO A. DELIBERIS

CHARLES STARK DRAPER LABORATORY, INC.
555 TECHNOLOGY SQUARE
CAMBRIDGE, MA 02139
01CY ATTN D. B. COX
01CY ATTN J. P. GILMORE MS 63

COMPUTER SCIENCES CORPORATION
P. O. BOX 530
6565 ARLINGTON BLVD
FALLS CHURCH, VA 22046
01CY ATTN H. BLANK
01CY ATTN JOHN SPOOR

COMSAT LABORATORIES
LINTHICUM ROAD
CLARKSBURG, MD 20734
01CY ATTN R. R. TAUR

CORNELL UNIVERSITY
DEPARTMENT OF ELECTRICAL ENGINEERING
ITHACA, NY 14850
01CY ATTN D. T. FARLEY JR

ESL INC.
495 JAVA DRIVE
SUNNYVALE, CA 94086
01CY ATTN R. K. STEVENS
01CY ATTN J. ROBERTS
01CY ATTN JAMES MARSHALL
01CY ATTN V. L. MOWER
01CY ATTN C. W. PRETTIE

FORD AEROSPACE & COMMUNICATIONS CORP
3939 FABIAN WAY
PALO ALTO, CA 94303
01CY ATTN J. T. MATTINGLEY MS X22

GENERAL ELECTRIC COMPANY
SPACE DIVISION
VALLEY FORGE SPACE CENTER
GODDARD BLVD KING OF PRUSSIA
P. O. BOX 8555
PHILADELPHIA, PA 19101
01CY ATTN M. H. BORTNER SPACE SCI LAB

GENERAL ELECTRIC COMPANY
TEMPO-CENTER FOR ADVANCED STUDIES
816 STATE STREET (P.O. DRAWER QQ)
SANTA BARBARA, CA 93102
01CY ATTN DASIAC
01CY ATTN DON CHANDLER
01CY ATTN TOM BARRETT
01CY ATTN TIM STEPHENS
01CY ATTN WARREN S. KNAPP
01CY ATTN WILLIAM MCNAMERA
01CY ATTN B. GAMBILL
01CY ATTN MACK STANTON

GENERAL RESEARCH CORPORATION
P. O. BOX 3587
SANTA BARBARA, CA 93105
01CY ATTN JOHN ISE JR
01CY ATTN JOEL GARBARINO

GEOPHYSICAL INSTITUTE
UNIVERSITY OF ALASKA
FAIRBANKS, AK 99701
(ALL CLASS ATTN: SECURITY OFFICER)
01CY ATTN T. N. DAVIS (UNCL ONLY)
01CY ATTN NEAL BROWN (UNCL ONLY)
01CY ATTN TECHNICAL LIBRARY

GTE SYLVANIA, INC.
ELECTRONICS SYSTEMS GRP-EASTERN DIV
77 A STREET
NEEDHAM, MA 02194
01CY ATTN MARSHAL CROSS

INSTITUTE FOR DEFENSE ANALYSES
400 ARMY-NAVY DRIVE
ARLINGTON, VA 22202
01CY ATTN J. M. AEIN
01CY ATTN ERNEST BAUER
01CY ATTN HANS WOLFHARD
01CY ATTN JOEL BENGSTEN

HARRIS CORP, E.S.D.
P. O. BOX 37
MELBOURNE, FL 32901
01CY ATTN ADV PROG DEPT DR. CARL DAVIS

HSS, INC.
2 ALFRED CIRCLE
BEDFORD, MA 01730
01CY ATTN DONALD HANSEN

INTL TEL & TELEGRAPH CORPORATION
500 WASHINGTON AVENUE
NUTLEY, NJ 07110
01CY ATTN TECHNICAL LIBRARY

JAYCOR
1401 CAMINO DEL MAR
DEL MAR, CA 92014
01CY ATTN S. R. GOLDMAN

JOHNS HOPKINS UNIVERSITY
APPLIED PHYSICS LABORATORY
JOHNS HOPKINS ROAD
LAUREL, MD 20810
01CY ATTN DOCUMENT LIBRARIAN
01CY ATTN THOMAS POTEMRA
01CY ATTN JOHN DASSOULAS

LOCKHEED MISSILES & SPACE CO INC
P. O. BOX 504
SUNNYVALE, CA 94088
01CY ATTN DEPT 60-12
01CY ATTN D. R. CHURCHILL

LOCKHEED MISSILES AND SPACE CO INC
3251 HANOVER STREET
PALO ALTO, CA 94304
01CY ATTN MARTIN WALT DEPT 52-10
01CY ATTN RICHARD G. JOHNSON DEPT 52-12
01CY ATTN BILLY M. MCCORMAC DEPT 52-54

KAMAN SCIENCES CORP
P. O. BOX 7463
COLORADO SPRINGS, CO 80933
01CY ATTN B. J. BITTNER

LINKABIT CORP
10453 ROSELLE
SAN DIEGO, CA 92121
01CY ATTN IRWIN JACOBS

M.I.T. LINCOLN LABORATORY
P. O. BOX 73
LEXINGTON, MA 02173
01CY ATTN LIB A-082 FOR DAVID M. TOWLE
01CY ATTN MR. WALDEN X113
01CY ATTN JAMES H. PANNELL L-246
01CY ATTN D. CLARK

MCDONNELL DOUGLAS CORPORATION
5301 BOLSA AVENUE
HUNTINGTON BEACH, CA 92647
01CY ATTN N. HARRIS
01CY ATTN J. MOULE
01CY ATTN GEORGE MROZ
01CY ATTN BILL OLSON

MISSION RESEARCH CORPORATION
735 STATE STREET
SANTA BARBARA, CA 93101
01CY ATTN P. FISCHER
01CY ATTN W. F. CREVIER
01CY ATTN STEVEN L. GUTSCHE
01CY ATTN D. SAPPENFIELD
01CY ATTN R. BOGUSCH
01CY ATTN R. HENDRICK
01CY ATTN RALPH KILB
01CY ATTN DAVE SOWLE
01CY ATTN F. FAJEN
01CY ATTN M. SCHEIBE
01CY ATTN CONRAD L. LONGMIRE
01CY ATTN WARREN A. SCHLUETER

MITRE CORPORATION, THE
P. O. BOX 208
BEDFORD, MA 01730
01CY ATTN J. C. KEENAN
01CY ATTN G. HARDING
01CY ATTN CHIEF SCIENTIST W. SEN
01CY ATTN S. A MORIN
01CY ATTN C. E. CALLAHAN

PACIFIC-SIERRA RESEARCH CORP
1456 CLOVERFIELD BLVD.
SANTA MONICA, CA 90404
01CY ATTN E. C. FIELD JR

PHOTOMETRICS, INC.
442 MARRETT ROAD
LEXINGTON, MA 02173
01CY ATTN IRVING L. KOFSKY

PHYSICAL DYNAMICS INC.
P. O. BOX 21589
SEATTLE, WA 98111
01CY ATTN E. J. FREMOUW

PHYSICAL DYNAMICS INC.
P. O. BOX 1069
BERKELEY, CA 94701
01CY ATTN A. THOMPSON
01CY ATTN JOSEPH B. WORKMAN

R & D ASSOCIATES
P. O. BOX 9695
MARINA DEL REY, CA 90291
01CY ATTN RICHARD LATTER
01CY ATTN FORREST GILMORE
01CY ATTN BRYAN GABBARD
01CY ATTN WILLIAM B. WRIGHT JR
01CY ATTN ROBERT F. LELEVIER
01CY ATTN WILLIAM J. KARZAS

RAND CORPORATION, THE
1700 MAIN STREET
SANTA MONICA, CA 90406
01CY ATTN CULLEN CRAIN
01CY ATTN ED BEDROZIAN

SCIENCE APPLICATIONS, INC.
P. O. BOX 2351
LA JOLLA, CA 92038
01CY ATTN LEWIS M. LINSON
01CY ATTN DANIEL A. HAMLIN
01CY ATTN D. SACHS
01CY ATTN E. A. STRAKER
01CY ATTN CURTIS A. SMITH
01CY ATTN JACK MCDOUGAL

RAYTHEON CO.
528 BOSTON POST ROAD
SUDBURY, MA 01776
01CY ATTN BARBARA ADAMS

SCIENCE APPLICATIONS, INC.
HUNTSVILLE DIVISION
2109 W. CLINTON AVENUE
SUITE 700
HUNTSVILLE, AL 35805
01CY ATTN DALE H. DIVIS

SCIENCE APPLICATIONS, INCORPORATED
8400 WESTPARK DRIVE
MCLEAN, VA 22101
01CY ATTN B. ADAMS

STANFORD RESEARCH INSTITUTE
333 RAVENSWOOD AVENUE
MENLO PARK, CA 94025
01CY ATTN DONALD NEILSON
01CY ATTN ALAN BURNS
01CY ATTN G. SMITH
01CY ATTN L. L. COBB
01CY ATTN DAVID A. JOHNSON
01CY ATTN WALTER G. CHESNUT
01CY ATTN CHARLES L. RINO
01CY ATTN WALTER JAYE
01CY ATTN M. BARON
01CY ATTN RAY L. LEADABRAND

SYSTEM DEVELOPMENT CORPORATION
4130 LINDEN AVENUE
DAYTON, OH 45432
01CY ATTN F. G. MEYER

TECHNOLOGY INTERNATIONAL CORP
75 WIGGINS AVENUE
BEDFORD, MA 01730
01CY ATTN W. P. BOQUIST

TRW DEFENSE & SPACE SYS GROUP
ONE SPACE PARK
REDONDO BEACH, CA 90278
01CY ATTN R. K. PLEBUCH R1-2078
01CY ATTN ROBERT M. WEBB R1-1150

VISIDYNE, INC.
19 THIRD AVENUE
NORTH WEST INDUSTRIAL PARK
BURLINGTON, MA 01803
01CY ATTN CHARLES HUMPHREY
01CY ATTN J. W. CARPENTER

Please distribute one copy to each of the following people:

Advanced Research Projects Agency (ARPA)
Strategic Technology Office
Arlington, Virginia

Capt. Donald M. LeVine

Naval Research Laboratory
Washington, D.C. 20375

Dr. P. Mange
Dr. E. Peterkin
Dr. R. Meier
Dr. E. Szuszczewicz -- Code 7127
Dr. Timothy Coffey -- Code 7700 (20 copies)
Dr. Jay P. Boris -- Code 7750 (100 copies)

Science Applications, Inc.
1250 Prospect Plaza
La Jolla, California 92037

Dr. D. A. Hamlin
Dr. L. Linson
Dr. D. Sachs

Director of Space and Environmental Laboratory
NOAA
Boulder, Colorado 80302

Dr. A. Glenn Jean
Dr. G. W. Adams
Dr. D. N. Anderson
Dr. K. Davies
Dr. R. F. Donnelly

A. F. Cambridge Research Laboratories
L. G. Hanscom Field
Bedford, Mass. 01730

Dr. T. Elkins
Dr. W. Swider
Mrs. R. Sagalyn
Dr. J. M. Forbes
Dr. T. J. Keneshea
Dr. J. Aarons

Office of Naval Research
800 North Quincy Street
Arlington, Virginia 22217

Dr. J. G. Dardis
Dr. H. Mullaney

Commander
Naval Electronics Laboratory Center
San Diego, California 92152

Dr. M. Bleiweiss
Dr. I. Rothmuller
Dr. V. Hildebrand
Mr. R. Rose

U. S. Army Aberdeen Research and Development Center
Ballistic Research Laboratory
Aberdeen, Maryland

Dr. F. Niles
Dr. J. Heimerl

Commander
Naval Air Systems Command
Department of the Navy
Washington, D. C. 20360

Dr. T. Czuba

Harvard University
Harvard Square
Cambridge, Mass.

Dr. M. B. McElroy
Dr. R. Lindzen

Pennsylvania State University
University Park, Pennsulvania 16802

Dr. J. S. Nisbet
Dr. P. R. Rohrbaugh
Dr. D. E. Baran
Dr. L. A. Carpenter
Dr. M. Lee
Dr. R. Divany
Dr. P. Bennett
Dr. E. Klevans

University of California, Los Angeles
405 Hillgard Avenue
La Jolla, California 90024

Dr. F. V. Coroniti
Dr. C. Kennel

University of California, Berkeley
Berkeley, California 94720

Dr. M. Hudson

Utah State University
4th N. and 8th Streets
Logan, Utah 84322

Dr. P. M. Banks
Dr. R. Harris
Dr. V. Peterson
Dr. R. Megill

Cornell University
Ithaca, New York 14850

Dr. W. E. Swartz
Dr. R. Sudan
Dr. D. Farley
Dr. M. Kelley
Dr. E. Ott

NASA
Goddard Space Flight Center
Greenbelt, Maryland 20771

Dr. S. Chandra
Dr. K. Maedo

Princeton University
Plasma Physics Laboratory
Princeton, New Jersey 08540

Dr. F. Perkins

Institute for Defense Analysis
400 Army/Navy Drive
Arlington, Virginia 22202

Dr. E. Bauer